Decomposing Polyclonal Sera using Neutralization Maps

Authors: Tal Einav[1]*, Adrian Creanga[2], Masaru Kanekiyo[2].

Affiliations

[1]Basic Sciences Division and Computational Biology Program, Fred Hutchinson Cancer Research Center, Seattle, Washington, United States of America.

[2]Vaccine Research Center, National Institute of Allergy and Infectious Diseases, National Institutes of Health, Bethesda, MD 20892, United States.

*Correspondence to: teinav@fredhutch.org

Abstract

Antibodies constitute a key line of defense against invading pathogens. Although monoclonal antibodies can be readily quantified in terms of their binding affinity, neutralization potential, and antigenic site, there has been limited success in characterizing the individual antibodies within polyclonal sera using these same metrics. This ability to dissect sera would provide a nuanced view into how our antibody repertoire evolves and help clarify whether a potent serum consists of a single dominant antibody or combines multiple antibodies. Using the neutralization data of monoclonal antibodies against the influenza virus, we develop a new form of antigenic cartography called a neutralization map that characterizes all possible antibody-virus interactions for the hemagglutinin head and stem. With these maps, the collective neutralization of polyclonal mixtures can be decomposed to determine the number of head and stem antibodies as well as their individual neutralization profiles. As a case study, we find that over 70% of ferrets infected with a single strain of influenza elicit a polyclonal antibody response, and we demonstrate that serum titers against a subset of viruses can predict the titers of the remaining viruses. Looking forward, we anticipate that this framework can be used to both visually and quantitatively assess changes in the neutralization capacity of polyclonal serum elicited by natural infection or vaccination.

Introduction

A key unsolved problem in immunology is to understand the functional characteristics of the antibodies within human serum and track how they change over time. With every infection or vaccination against the influenza virus, our antibody repertoire is reshaped, leading to a complex immune landscape whose ability to protect us from past and current strains is difficult to quantify (*1*, *2*). While much effort has been devoted to the reverse problem, namely, characterizing individual antibodies and predicting the effectiveness of their combinations (*3–5*), unweaving the thread of antibodies within serum is intractable without a framework to enumerate the spectrum of antibody-virus interactions. Here, we create such a framework, opening up a unique perspective to quantify and understand polyclonal sera.

To that end, we develop a new method based on the techniques of antigenic cartography and antibody fingerprinting to characterize how well individual antibodies can neutralize a panel of influenza viruses. Antigenic cartography transforms hemagglutination inhibition data (the ability to inhibit virus binding) of a person's or animal's serum into a map of virus-serum interactions (*6*, *7*). While this technique imposes a structure for how sera can behave, it is unable to characterize the antibodies within a given serum nor predict the level of inhibition offered by different combinations of sera. Moreover, current techniques are restricted (via the hemagglutination inhibition data they use) to characterizing antibodies binding to the head of influenza hemagglutinin (HA) and thus far remain ignorant of other antigenic sites.

A complementary method that partially offsets these drawbacks is antibody fingerprinting, where the neutralization profiles of large panels of antibodies are clustered to identify virus neutralization patterns or "fingerprints" (*8*). Applying this process in reverse can decompose polyclonal sera into their constitutive antibodies, although this decomposition is limited to the antibodies in the original panel or to guessing novel antibody signatures (*9*). Moreover, as with antigenic cartography, these fingerprints have thus far not directly incorporated information on antibody epitopes.

In this work, we draw inspiration from both antigenic cartography and antibody fingerprinting to create monoclonal antibody neutralization maps against a panel of influenza viruses (Figure 1A,B). By shifting the focus from sera to monoclonal antibodies, we create maps that quantify neutralization in absolute units for the head and stem of influenza HA. These maps define an underlying structure for antibody-virus interactions, enabling us to decompose a polyclonal serum and predict the number of antibodies within it as well as their neutralization profiles (Figure 1C). Performing this decomposition on as few as 5 viruses predicts the mixture neutralization against all other viruses on the map. Overall, this methodology can serve as a stepping stone to quantify how human serum changes over time.

Using monoclonal antibody data to create neutralization maps of the hemagglutinin head and stem.

Antigenic cartography utilizes metric multidimensional scaling (MDS) to coalesce individual interactions (the ability of one antibody to inhibit one virus strain) into a global map (*10*). As a helpful geographic analogy, MDS can transform a table of pairwise distances between cities to create a state map (Figure S1). When cities are replaced by viruses and antibodies, the same

procedure generates a map where the concentration of serum required to neutralize a virus is solely dictated by its distance to that virus, with smaller distances signifying more potent sera.

We utilized a panel of influenza viruses containing 15 H1N1 strains collected between 1933-2008 and 21 H3N2 strains collected from 1968-2016 (Figure S2) (*11*). The concentration of each antibody needed to neutralize every virus by 50% (the half maximal inhibitory concentration, IC_{50}) was determined for 6 HA head-binding and 12 HA stem-binding antibodies representing major lineages of broadly neutralizing antibodies elicited by vaccination (*12*, *13*). HA head and stem maps were constructed using their respective sets of antibodies, and on each map only the relative distance (and not the angle or absolute coordinates) between an antibody and virus dictates the antibody's potency (Figure 1A). As more viruses and antibodies are added, they lock into a fixed configuration, aside from global translations, rotations, and reflections.

Using the IC_{50} values of each antibody-virus pair, we first performed outlier detection and then created the two neutralization maps shown in Figure 1B [SI Methods]. A distance d on the map translates into an IC_{50} of 10^{-10+d} Molar (with 1 μg/mL = $6.6 \cdot 10^{-9}$ M for the IgG antibodies considered here), so that greater distance represents exponentially decreasing inhibitory action.

These head and stem maps visually demonstrate the difference between antibodies binding to different regions of HA. In the stem map, the H1N1 strains and H3N2 strains each fit inside a circle of radius 1.0 (in map distance units), implying that the most cross-reactive stem-binding antibody (placed at the center of each circle) would have an $IC_{50} \leq 10^{-9}$ M (0.2 μg/mL) against any of these strains. In contrast, on the HA head map the H1N1 and H3N2 strains are more dispersed, lying within circles of radii 2.4 and 1.9, respectively. Hence, the most cross-reactive head antibody targeting all H1N1 strains could only have an $IC_{50} \leq 10^{-7.6}$ M (4 μg/mL) while an antibody targeting all H3N2 strains could have an $IC_{50} \leq 10^{-8.1}$ M (1 μg/mL). In summary, these maps not only visually demonstrate that the HA stem is more conserved than the head, but can quantify to what extent neutralization will occur for any antibody.

Since these neutralization maps attempt to translate the complex and potentially highly-multidimensional antibody-virus interactions into 2D, and it is possible that no such low-dimensional representation exists. After creating our head and stem maps, we quantified their accuracy by computing the fold-error between the map IC_{50} and measured IC_{50} for all antibody-virus pairs, with a lower limit of $\langle \text{error} \rangle$=1x for a map that perfectly represents the data [SI methods]. We find that the head map has an $\langle \text{error} \rangle$=2.2x (i.e. at least 50% of antibody-virus IC_{50} values are within this error range, so that an $IC_{50}=10^{-8}$ M typically lies between (10^{-8} M)/2.2 and (10^{-8} M)·2.2 on the map) while the stem map has an $\langle \text{error} \rangle$=1.5x. Surprisingly, the error only decreases by 5% in 3D, although it more than doubles in 1D (Figure S3). Hence, as with antigenic cartography (*6*), we opt to represent the data in 2D which offers a balanced tradeoff between the ease of visualization and the accuracy of the maps.

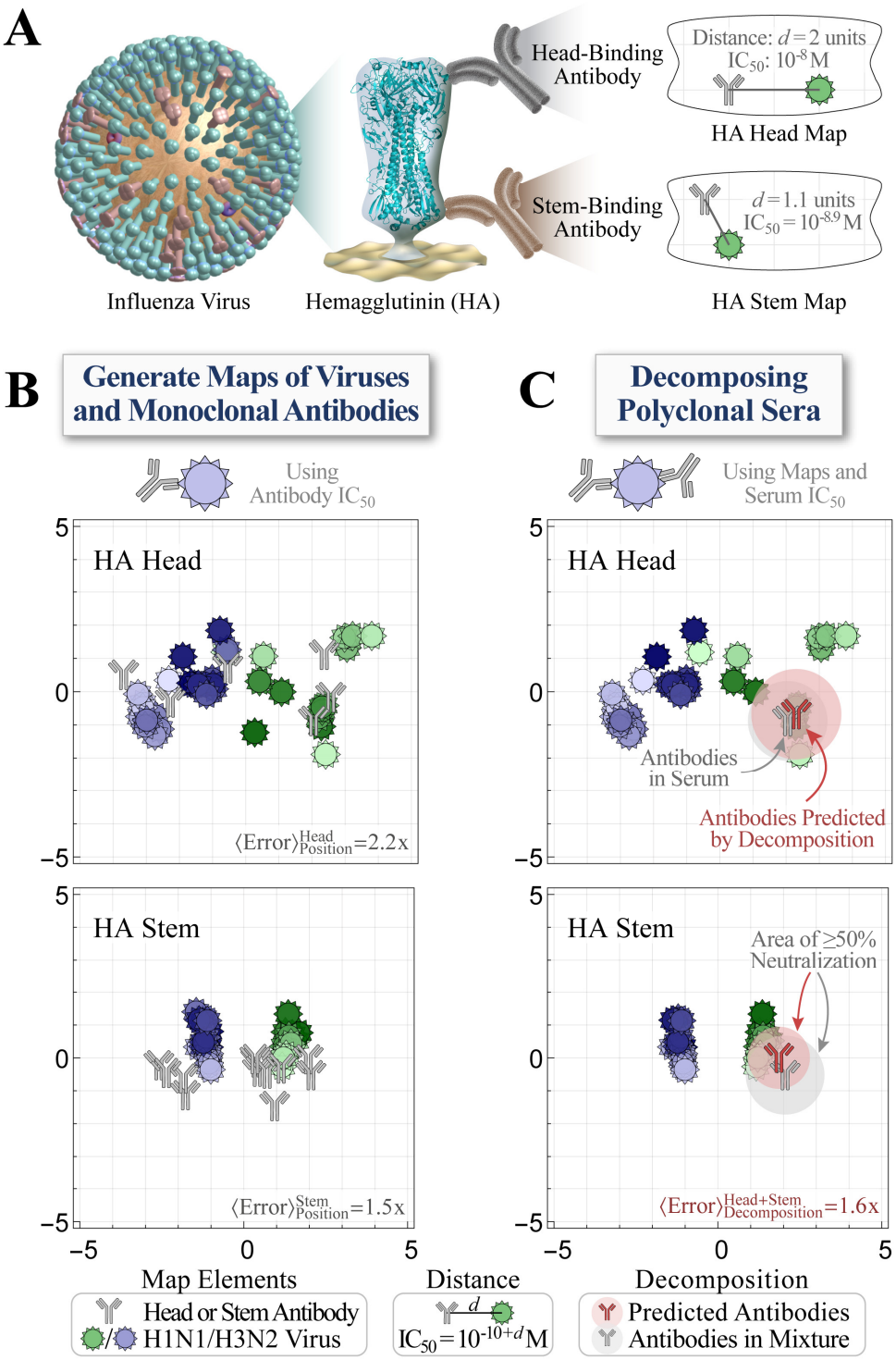

Fig. 1. Neutralization maps of the HA head and stem. (A) Antibodies targeting the HA head or stem were used to map these two regions. (B) Neutralization maps were generated using neutralization data from monoclonal antibodies (gray) against a panel of viruses (hues of green/blue) (*11*). The axes show the units of the grid, and the distance *d* between each antibody-virus pair corresponds to neutralization, where positive distance *d* represents an $IC_{50}=10^{-10+d}$ M while 0 distance represents any $IC_{50}\leq10^{-10}$ M. A complete list of virus strains is given in Figure S2. (C) 10 mixtures of two or three antibodies were created to test the decomposition algorithm. One such mixture is shown (gray; mixture #4 in Figure S4) together with the predicted decomposition (red). The

disk surrounding each antibody represents the region of ≥50% neutralization when the total mixture concentration equals a fixed amount we chose as $10^{-8.5}$ Molar [SI Methods]. The errors for the head and stem map in Panel B represent the discrepancy between the map and actual antibody-virus IC_{50} values, whereas the error in Panel C denotes the discrepancy of the predicted mixture (including both the head and stem antibody) and the actual mixture IC_{50} values.

Decomposing the number and functional characteristics of antibodies within mixtures.
These maps enumerate the possible neutralization profiles of an arbitrary antibody, providing the means to unravel the distinct signatures within a polyclonal mixture. Utilizing only the neutralization data of a mixture (with no knowledge of the number of antibodies or their individual neutralization profiles), the algorithm scans through all possible configurations of antibodies on the map and determines which one best describes the mixture (Figures S4-S6), terminating once the error no longer appreciably decreases with additional antibodies [SI Methods]. In other words, we use an Occam's razor approach to describe each mixture using the smallest possible set of antibodies that display the correct neutralization profile. Unlike antibody fingerprinting (*8*), this decomposition is not limited to the neutralization profiles of the antibodies within our panel but instead aims to characterize the behavior of any antibody against influenza.

We tested our decomposition algorithm on two sets of polyclonal mixtures. We first created 10 mixtures containing either two or three antibodies from our panel and measured their collective neutralization against the viruses on our neutralization maps. Since each antibody was individually characterized, we can compare these decompositions against the true mixture compositions. We next tested our algorithm on polyclonal ferret sera elicited by influenza infection. These sera undoubtedly include antibodies outside our panel and therefore assess how well we capture general antibody-virus interactions.

As an example decomposition, Figure 1C shows one of our antibody mixtures containing 1 head and 1 stem antibody from our panel with a 50%/50% composition (gray; mixture #4 in Figure S4). The algorithm predicted that this mixture contained 1 head and 1 stem antibody with a 70%/30% composition (Figures S7-S9) [SI Methods]. Beyond the number and fraction of each antibody, the locations (and hence the neutralization profiles) of the predicted antibodies closely match the actual antibodies in the mixture. The slight deviations between the predicted and actual coordinates is partially compensated by predicting an uneven composition, so that the resulting decomposition accurately describes the true mixture behavior. The average discrepancy between the measured and predicted mixture IC_{50} values is 1.6x, which includes the collective neutralization from the head and stem antibodies. The disks surrounding each antibody represent the region of ≥50% neutralization when the total mixture concentration equals a fixed amount we chose as $10^{-8.5}$ Molar [SI Methods], and the viruses covered by these regions are very similar between the predicted and actual mixtures.

Determining whether a mixture of antibodies is monoclonal or polyclonal.
One application of the neutralization maps is to determine whether an unknown mixture contains a single dominant antibody or multiple distinct antibodies. The decomposition algorithm relies on detecting polyclonal antibody signatures that are impossible for a monoclonal antibody to achieve. For example, if a mixture exhibits an $IC_{50}<10^{-9}$ Molar against two viruses more than 2

units apart on a map, that mixture cannot be composed of a single antibody which would need to be within d=1 unit ($IC_{50}=10^{-10+d}$ Molar) of each virus (Figure 2A, left).

Another application of the neutralization maps is to determine the precise number and neutralization properties (map locations) of the antibodies within a mixture. When measurements against more viruses are included, the error markedly decreases when the correct polyclonal decomposition is found (Figure 2A, right).

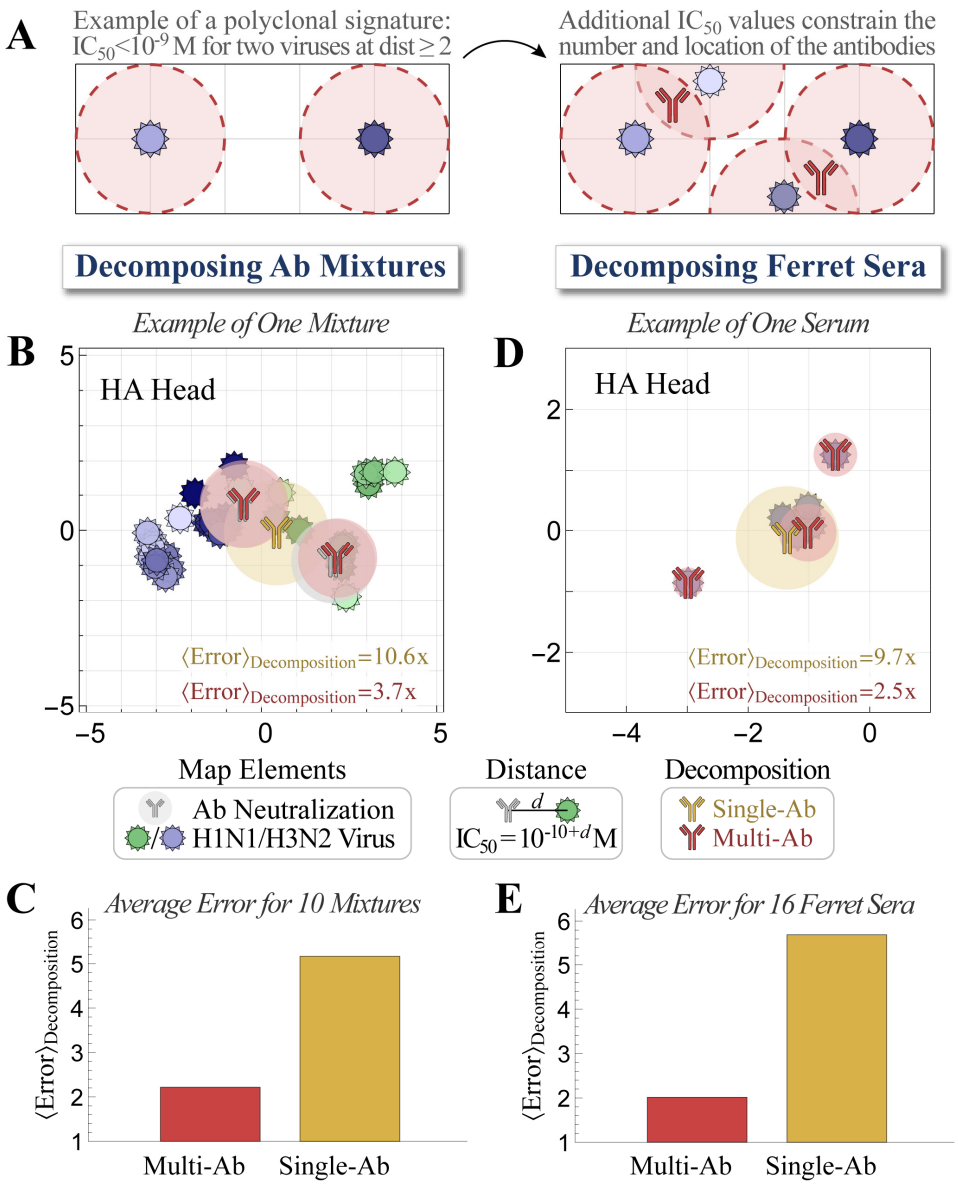

Fig. 2. Decomposing antibody mixtures based on neutralization or HAI data. (A) Combinations of antibodies can exhibit neutralization signatures that are not possible for monoclonal antibodies. (B) Neutralization data from 10 antibody mixtures were created to test the decomposition algorithm. An example decomposition is shown for a mixture containing 2 head antibodies (gray; mixture #1 in Figure S4) which lie right below the predictions of a multi-antibody decomposition (red). In contrast, a decomposition that only considers a single head-targeting antibody (gold) exhibits a larger error. (C) The average error for the 10 antibody

mixtures using a multi-antibody or single-antibody decomposition [SI Methods]. (D) The sera of ferrets infected with a single virus strain were decomposed using their HAI data and the HA head map (*7*). A multi-antibody (red) or single-antibody (gold) decomposition is shown for a ferret infected with A/Wyoming/3/2003. (E) The average error for 16 ferret sera exhibiting polyclonal signatures.

To demonstrate how well polyclonal antibody signatures can be distinguished from monoclonal signatures, we analyzed our 10 mixtures where the number and properties of the underlying antibodies are known. Figure 2B displays a mixture containing 2 head antibodies (gray, partially obscured under the red antibodies; mixture #1 in Figure S4). We first decomposed this mixture using the multi-antibody model, where the number of antibodies is unconstrained (and hence the decomposition can contain one or more antibodies). Without prior knowledge of the mixture composition, the algorithm predicted two head antibodies (red) that lie on top of the actual antibody positions with an error of 3.1x. In contrast, using a single-antibody decomposition that is forced to use one head antibody (gold), the error increases to 10.6x as the single antibody tries to mimic the neutralization capabilities of two distinct antibodies.

Figure 2C shows the results of our decomposition algorithm when applied to all 10 antibody mixtures (Figure S9). The unconstrained multi-antibody decompositions had an average error of 2.3x, while forcing each decomposition to use a single antibody increased the average error to 5.2x (Figures S10-S11) [SI methods]. In summary, unknown mixtures of antibodies can be decomposed using the neutralization maps. Whereas antigenic cartography has traditionally represented both monoclonal antibodies and antibody mixtures as single points (*6*), we find that antibody mixtures can be more accurately decomposed using multiple points (one per antibody).

Ferrets infected with a single virus strain can produce a polyclonal antibody response. We next applied the decomposition algorithm to examine ferret sera whose antibody composition is not known. Specifically, we set out to test the classic assumption that animals infected with a single influenza strain may elicit a mostly monoclonal antibody response (*6*, *14*, *15*). Sera from these animals is used in influenza surveillance to characterize the antigenicity of new strains by measuring a serum's HAI titer (the maximum dilution of serum that can inhibit the hemagglutination of a virus). Antigenic cartography characterizes such sera as single points on a map (i.e. as monoclonal antibodies within our framework), and if a sizable fraction of sera is polyclonal, this could distort the map structure.

We considered HAI measurements of 22 ferret sera individually assessed against a large array of H3N2 viruses (*7*). Nine of these viruses overlapped with our panel, enabling us to apply our decomposition algorithm [SI Methods]. Since the HAI assay only quantifies head-binding antibodies, we restrict our analysis to the HA head map.

After infection by a single strain of influenza, 16 out of 22 (73%) ferret sera exhibited a polyclonal response containing at least two distinct antibodies (Figures S12-S13). An example is shown in Figure 2D for serum elicited by infection with H3N2 A/Wyoming/3/2003. The best multi-antibody decomposition characterized this mixture using three head antibodies (red), resulting in an error of 2.5x, whereas decomposing this mixture as a single antibody (gold) increased the error to 9.7x. Overall, the 16 sera with polyclonal signatures had an average error of 2.0x for multi-antibody decompositions compared to an average error of 5.7x when forcing a

single-antibody decomposition (Figure 2E), comparable to the analysis of our antibody mixtures in Figure 2C. While we cannot directly validate these individual antibodies (as was possible for our antibody mixtures), we next discuss how decomposition on a subset of the serum measurements accurately predicts the remaining measurements, demonstrating that our neutralization maps capture the virus-antibody interactions within these ferret sera.

Decomposing a subset of viruses enables prediction of out-of-sample viruses.
Since sera are not assessed against a standardized panel of viruses, it is difficult to compare sera or understand the reasons behind any differences in neutralization. Moreover, since the supply of each serum is inherently limited, a standardized panel would ideally require a minimal number of measurements from which the serum's behavior against other viruses could be extrapolated. Given the small error achieved when decomposing our antibody mixtures using the full 33 virus panel, we investigated whether a decomposition performed using a smaller number of viruses could enable robust predictions against the remaining viruses (Figure 3A).

We selected 5 virus strains (H1N1 A/New Jersey/8/1976, H1N1 A/New York/638/1995, H1N1 A/Canterbury/76/2000, H3N2 A/Texas/1/1977, H3N2 A/Victoria/361/2011) that were spread out across the HA head and stem maps (Figure S2) to ensure that an antibody anywhere on the maps could be accurately placed. We then applied our decomposition algorithm using only these 5 viruses and quantified the error between the predicted IC_{50} and experimentally measured IC_{50} for the remaining 28 viruses.

Figure 3B shows a decomposition of the same mixture from Figure 2B, using only the neutralization data from our 5 selected strains (red) and without any knowledge of the number of antibodies in the mixture or their neutralization properties. While decomposing on this limited set of data predicted three (instead of two) head antibodies, the prediction error arising from these three antibodies was only 5.7x against the remaining 28 out-of-sample viruses (gray). Note that the decomposition error used in Figure 2 characterized how well a mixture's neutralization data could be represented on the map, whereas the prediction error we now consider only compares the predicted and measured IC_{50}s for viruses *not* used in the decomposition.

The mean prediction error from applying this limited decomposition across all 10 antibody mixtures is shown in Figure 3C, with an average prediction error of 3.4x for multi-antibody decompositions (Figure S14). As above, we also assessed the traditional antigenic cartography approach of modeling antibody mixtures as single points which resulted in an average prediction error of 5.5x.

Notably, both the multi- and single-antibody prediction errors are only marginally larger than the decomposition errors using the full suite of data in Figure 2C. This suggests that additional measurements minimally improve a decomposition performed on a small but well-dispersed subset of viruses. Given that these five measurements must determine the number of antibodies, their locations on the map, and their fractional compositions, this low prediction error highlights the wealth of information encoded by the virus locations on a neutralization map.

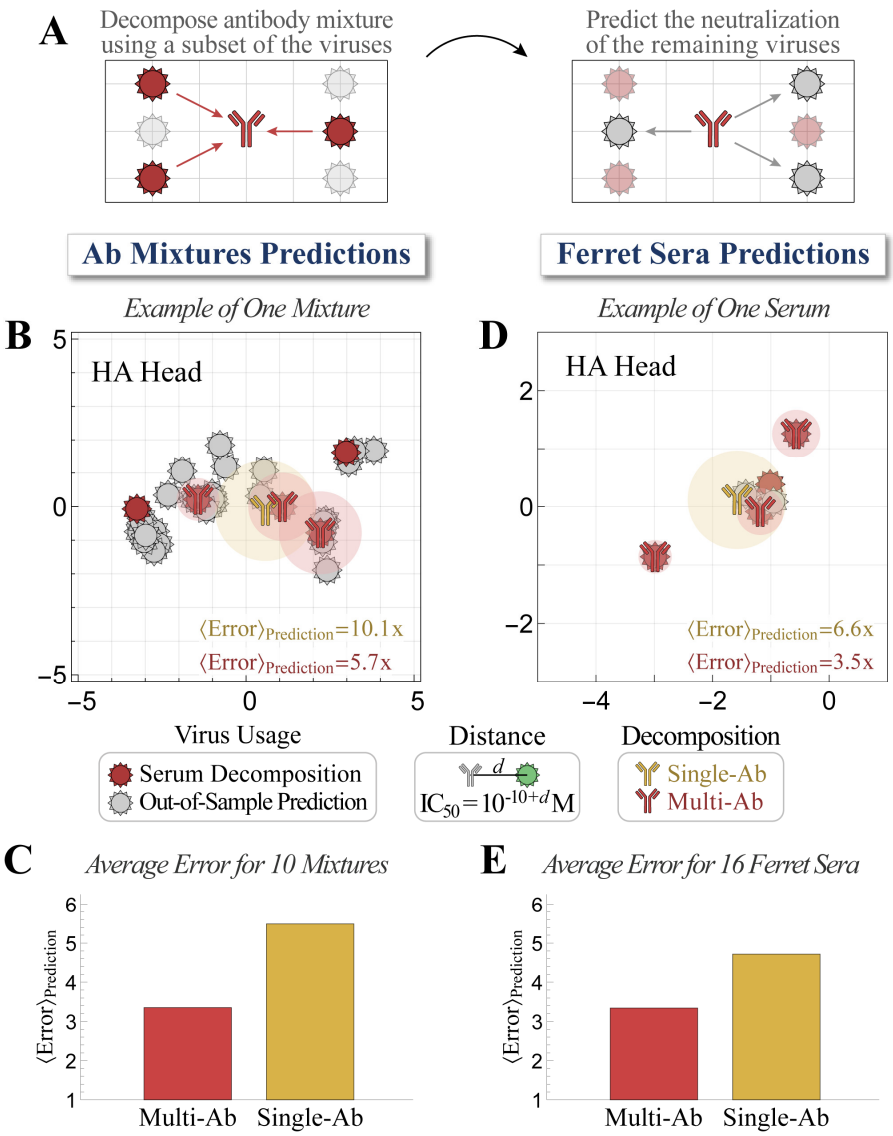

Fig. 3. Decomposing antibody mixtures on a subset of viruses predicts their effectiveness against the remaining viruses. (A) Antibody mixtures were decomposed using a subset of strains (red) to predict the response against all other viruses on the map (gray). (B,D) Example multi-antibody (red) and single-antibody (gold) decompositions for the same mixture and serum from Figure 2B,D, but using data from a subset of viruses for decomposition. The error compares the measured and predicted IC_{50} of the out-of-sample viruses. For simplicity, all viruses used for decomposition are shown in red while the remaining viruses used for prediction are shown in gray. (C,E) The prediction error for all antibody mixtures or ferret sera.

We next repeated our analysis using the ferret sera, performing the decomposition on subsets of 3 to 5 viruses spread out across the map [SI Methods]. Figure 3D shows an example decomposition performed on the same serum from Figure 2D, using only four viruses for the decomposition (red). Overall, the 16 ferret sera with polyclonal signatures resulted in a mean prediction error of 3.3x using multi-antibody decompositions (on par with the antibody mixture data), while single-antibody decompositions resulted in a slightly larger mean prediction error of 4.7x (Figure 3E).

Discussion

In summary, we have presented an expanded form of antigenic cartography based on the neutralization data of monoclonal antibodies against a panel of influenza strains. By building these maps using monoclonal antibodies, the fundamental units of an antibody repertoire, we created a more refined representation of different antigenic sites such as the HA head and stem where map distance directly translates into absolute units of antibody concentration (Figure 1).

The structure of these maps enables us to decompose polyclonal mixtures of antibodies – even for antibodies not included in our original panel – and quantify their fractional composition and neutralization profiles (Figure 2). Hence, these maps can utilize neutralization or hemagglutination inhibition assays to quantify what fraction of polyclonal sera target the HA head or stem and track how this response evolves in time, providing a complementary method to direct experimental techniques such as mutating binding epitopes (*16*) or sequencing and recombinantly expressing antibodies (*17–19*). Decomposition could also be used to create the best approximation of a serum sample by combining the closest known antibodies to each point in its decomposition, providing a way to rationally design a serum and circumvent its inherently limited supply.

Our analysis assumes that our maps contain a sufficient number of antibodies to capture the interactions between a general antibody and the influenza virus. While this assumption does not require a monoclonal antibody with every possible neutralization profile to be present in our panel, having too few antibodies will diminish the resolution of a map. For example, both the H1N1 A/WSN/1933 and H3N2 A/Fujian/411/2002 strains show identical neutralization profiles against the six HA head antibodies and consequently have similar coordinates near (-0.6,1.2) in the HA head map (Figure S2). While rare antibodies can inhibit both H1N1 and H3N2 viruses (*18*, *20*), if an antibody exists that neutralizes these two strains differently, it would split up the locations of these two viruses.

Another limitation of the decomposition algorithm is that antibodies comprising a small fraction of a mixture will minimally affect its neutralization and hence cannot be reliably detected [SI Methods]. Moreover, if a mixture contains antibodies that lie close together on a map (and hence have very similar neutralization profiles), they would be decomposed as a single antibody. Hence, decomposing polyclonal ferret or human sera may yield antibody signatures representing amalgams of similar antibodies, but this decomposition would nevertheless accurately capture the functional response of this serum against influenza.

For example, our multi-antibody decomposition algorithm characterized the HAI profiles of ferret sera with 2x error, which equals the inherent error of the HAI assay (Figure 2E). These ferrets must produce antibodies that were not in our original panel of human antibodies, demonstrating that we can extrapolate to antibody behaviors outside of our panel (*9*). Moreover, for both our designed antibody mixtures and the ferret sera, each mixture's ability to inhibit or neutralize a subset of viruses was sufficient to predict its potency against the remaining viruses on a map, provided this subset was dispersed along the map (Figure 3).

Looking forward, our analysis of simple antibody mixtures presented here serves as a stepping stone to quantify more complex polyclonal sera from ferrets infected with multiple strains and

humans with a far richer infection history. By decomposing longitudinal serum samples taken after multiple infections, we can quantify whether the antibody repertoire broadens or becomes more focused over time and shed light on how broadly neutralizing antibodies develop (*19*, *21*, *22*). Measurements of sera pre- and post-vaccination can enable us to visually analyze how drastically the antibody response is reshaped and how long such protection lasts (*23–25*). This analysis provides a new perspective to understand how our antibody repertoire interacts with pathogens and evolves over the course of our lives.

References and Notes

1. L. A. VanBlargan, L. Goo, T. C. Pierson, Deconstructing the antiviral neutralizing-antibody response: implications for vaccine development and immunity. *Microbiol. Mol. Biol. Rev.* **80**, 989–1010 (2016).

2. F. Krammer, The human antibody response to influenza a virus infection and vaccination. *Nat. Rev. Immunol.* **19** (2019), pp. 383–397.

3. M. M. Grandal, S. Havrylov, T. T. Poulsen, K. Koefoed, A. Dahlman, G. R. Galler, P. Conrotto, S. Collins, K. W. Eriksen, D. Kaufman, G. F. V. Woude, H. J. Jacobsen, I. D. Horak, M. Kragh, J. Lantto, T. Bouquin, M. Park, M. W. Pedersen, Simultaneous targeting of two distinct epitopes on met effectively inhibits met- and hgf-driven tumor growth by multiple mechanisms. *Mol. Cancer Ther.* **16**, 2780–2791 (2017).

4. K. A. Howell, J. M. Brannan, C. Bryan, A. McNeal, E. Davidson, H. L. Turner, H. Vu, S. Shulenin, S. He, A. Kuehne, A. S. Herbert, X. Qiu, B. J. Doranz, F. W. Holtsberg, A. B. Ward, J. M. Dye, M. J. Aman, Cooperativity enables non-neutralizing antibodies to neutralize ebolavirus. *Cell Rep.* **19**, 413–424 (2017).

5. N. S. Laursen, R. H. E. Friesen, X. Zhu, M. Jongeneelen, S. Blokland, J. Vermond, A. van Eijgen, C. Tang, H. van Diepen, G. Obmolova, M. van der Neut Kolfschoten, D. Zuijdgeest, R. Straetemans, R. M. B. Hoffman, T. Nieusma, J. Pallesen, H. L. Turner, S. M. Bernard, A. B. Ward, J. Luo, L. L. M. Poon, A. P. Tretiakova, J. M. Wilson, M. P. Limberis, R. Vogels, B. Brandenburg, J. A. Kolkman, I. A. Wilson, Universal protection against influenza infection by a multidomain antibody to influenza hemagglutinin. *Science.* **362**, 598–602 (2018).

6. D. J. Smith, A. S. Lapedes, J. C. de Jong, T. M. Bestebroer, G. F. Rimmelzwaan, A. D. M. E. Osterhaus, R. A. M. Fouchier, Mapping the antigenic and genetic evolution of influenza virus. *Science.* **305**, 371–376 (2004).

7. J. M. Fonville, S. H. Wilks, S. L. James, A. Fox, M. Ventresca, M. Aban, L. Xue, T. C. Jones, N. M. H. Le, Q. T. Pham, N. D. Tran, Y. Wong, A. Mosterin, L. C. Katzelnick, D. Labonte, T. T. Le, G. van der Net, E. Skepner, C. A. Russell, T. D. Kaplan, G. F. Rimmelzwaan, N. Masurel, J. C. de Jong, A. Palache, W. E. P. Beyer, Q. M. Le, T. H. Nguyen, H. F. L. Wertheim, A. C. Hurt, A. D. M. E. Osterhaus, I. G. Barr, R. A. M. Fouchier, P. W. Horby, D. J. Smith, Antibody landscapes after influenza virus infection or vaccination. *Science.* **346**, 996–1000 (2014).

8. I. S. Georgiev, N. A. Doria-Rose, T. Zhou, Y. Do Kwon, R. P. Staupe, S. Moquin, G. Y. Chuang, M. K. Louder, S. D. Schmidt, H. R. Altae-Tran, R. T. Bailer, K. McKee, M. Nason, S. O'Dell, G. Ofek, M. Pancera, S. Srivatsan, L. Shapiro, M. Connors, S. A. Migueles, L. Morris, Y. Nishimura, M. A. Martin, J. R. Mascola, P. D. Kwong, Delineating antibody recognition in polyclonal sera from patterns of hiv-1 isolate neutralization. *Science.* **340**, 751–756 (2013).

9. N. A. Doria-Rose, H. R. Altae-Tran, R. S. Roark, S. D. Schmidt, M. S. Sutton, M. K. Louder, G.-Y. Chuang, R. T. Bailer, V. Cortez, R. Kong, K. McKee, S. O'Dell, F. Wang, S. S. Abdool Karim, J. M. Binley, M. Connors, B. F. Haynes, M. A. Martin, D. C. Montefiori, L. Morris, J. Overbaugh, P. D. Kwong, J. R. Mascola, I. S. Georgiev, Mapping polyclonal hiv-1 antibody responses via next-generation neutralization fingerprinting. *PLOS Pathog.* **13**, e1006148 (2017).

10. A. Lapedes, R. Farber, The geometry of shape space: application to influenza. *J. Theor. Biol.* **212**, 57–69 (2001).

11. A. Creanga, R. A. Gillespie, B. E. Fisher, S. F. Andrews, L. Hatch, T. Stephens, Y. Tsybovsky, M. C. Crank, A. B. McDermott, J. R. Mascola, B. S. Graham, M. Kanekiyo, *bioRxiv*, in press, doi:10.1101/2020.02.24.963611.

12. M. G. Joyce, A. K. Wheatley, P. V. Thomas, G.-Y. Chuang, C. Soto, R. T. Bailer, A. Druz, I. S. Georgiev, R. A. Gillespie, M. Kanekiyo, W.-P. Kong, K. Leung, S. N. Narpala, M. S. Prabhakaran, E. S. Yang, B. Zhang, Y. Zhang, M. Asokan, J. C. Boyington, T. Bylund, S. Darko, C. R. Lees, A. Ransier, C.-H. Shen, L. Wang, J. R. Whittle, X. Wu, H. M. Yassine, C. Santos, Y. Matsuoka, Y. Tsybovsky, U. Baxa, J. C. Mullikin, K. Subbarao, D. C. Douek, B. S. Graham, R. A. Koup, J. E. Ledgerwood, M. Roederer, L. Shapiro, P. D. Kwong, J. R. Mascola, A. B. McDermott,

Vaccine-induced antibodies that neutralize group 1 and group 2 influenza a viruses. *Cell*. **166**, 609–623 (2016).

13. S. F. Andrews, M. J. Chambers, C. A. Schramm, J. Plyler, J. E. Raab, M. Kanekiyo, R. A. Gillespie, A. Ransier, S. Darko, J. Hu, X. Chen, H. M. Yassine, J. C. Boyington, M. C. Crank, G. L. Chen, E. Coates, J. R. Mascola, D. C. Douek, B. S. Graham, J. E. Ledgerwood, A. B. McDermott, Activation dynamics and immunoglobulin evolution of pre-existing and newly generated human memory b cell responses to influenza hemagglutinin. *Immunity*. **51**, 398-410.e5 (2019).

14. R. Lambkin, L. McLain, S. E. Jones, S. L. Aldridge, N. J. Dimmock, Neutralization escape mutants of type a influenza virus are readily selected by antisera from mice immunized with whole virus: a possible mechanism for antigenic drift. *J. Gen. Virol.* **75**, 3493–3502 (1994).

15. R. Lambkin, N. J. Dimmock, All rabbits immunized with type a influenza virions have a serum haemagglutination-inhibition antibody response biased to a single epitope in antigenic site b. *J. Gen. Virol.* **76**, 889–897 (1995).

16. D. Angeletti, J. S. Gibbs, M. Angel, I. Kosik, H. D. Hickman, G. M. Frank, S. R. Das, A. K. Wheatley, M. Prabhakaran, D. J. Leggat, A. B. McDermott, J. W. Yewdell, Defining b cell immunodominance to viruses. *Nat. Immunol.* **18**, 456–463 (2017).

17. F. Horns, C. Vollmers, C. L. Dekker, S. R. Quake, Signatures of selection in the human antibody repertoire: selective sweeps, competing subclones, and neutral drift. *Proc. Natl. Acad. Sci. U. S. A.* **116**, 1261–1266 (2019).

18. J. Lee, D. R. Boutz, V. Chromikova, M. G. Joyce, C. Vollmers, K. Leung, A. P. Horton, B. J. DeKosky, C.-H. Lee, J. J. Lavinder, E. M. Murrin, C. Chrysostomou, K. H. Hoi, Y. Tsybovsky, P. V Thomas, A. Druz, B. Zhang, Y. Zhang, L. Wang, W.-P. Kong, D. Park, L. I. Popova, C. L. Dekker, M. M. Davis, C. E. Carter, T. M. Ross, A. D. Ellington, P. C. Wilson, E. M. Marcotte, J. R. Mascola, G. C. Ippolito, F. Krammer, S. R. Quake, P. D. Kwong, G. Georgiou, Molecular-level analysis of the serum antibody repertoire in young adults before and after seasonal influenza vaccination. *Nat. Med.* **22**, 1456–1464 (2016).

19. J. Lee, P. Paparoditis, A. P. Horton, A. Frühwirth, J. R. McDaniel, J. Jung, D. R. Boutz, D. A. Hussein, Y. Tanno, L. Pappas, G. C. Ippolito, D. Corti, A. Lanzavecchia, G. Georgiou, Persistent antibody clonotypes dominate the serum response to influenza over multiple years and repeated vaccinations. *Cell Host Microbe*. **25**, 367-376.e5 (2019).

20. H. Zhang, C. Henry, C. S. Anderson, A. Nogales, M. L. Dediego, J. Bucukovski, L. Martinez-Sobrido, P. C. Wilson, D. J. Topham, B. L. Miller, Crowd on a chip: label-free human monoclonal antibody arrays for serotyping influenza. *Anal. Chem.* **90**, 9583–9590 (2018).

21. D. M. Skowronski, C. Chambers, G. De Serres, S. Sabaiduc, A.-L. Winter, J. A. Dickinson, J. B. Gubbay, K. Fonseca, S. J. Drews, H. Charest, C. Martineau, M. Krajden, M. Petric, N. Bastien, Y. Li, D. J. Smith, Serial vaccination and the antigenic distance hypothesis: effects on influenza vaccine effectiveness during a(h3n2) epidemics in canada, 2010–2011 to 2014–2015. *J. Infect. Dis.* **215**, 1059–1099 (2017).

22. E. P. Plant, L. J. Fredell, B. A. Hatcher, X. Li, M.-J. Chiang, M. Kosikova, H. Xie, O. Zoueva, A. A. Cost, Z. Ye, M. J. Cooper, Different repeat annual influenza vaccinations improve the antibody response to drifted influenza strains. *Sci. Rep.* **7**, 5258 (2017).

23. J. H. Kim, I. Skountzou, R. Compans, J. Jacob, Original antigenic sin responses to influenza viruses. *J. Immunol.* **97**, 177–183 (2009).

24. H. Q. McLean, M. G. Thompson, M. E. Sundaram, J. K. Meece, D. L. McClure, T. C. Friedrich, E. A. Belongia, Impact of repeated vaccination on vaccine effectiveness against influenza a(h3n2) and b during 8 seasons. *Clin. Infect. Dis.* **59**, 1375–1385 (2014).

25. M. G. Thompson, A. Naleway, A. M. Fry, S. Ball, S. M. Spencer, S. Reynolds, S. Bozeman, M. Levine, J. M. Katz, M. Gaglani, Effects of repeated annual inactivated influenza vaccination among healthcare personnel on serum hemagglutinin inhibition antibody response to a/perth/16/2009 (h3n2)-like virus during 2010-11. *Vaccine*. **34**, 981–988 (2016).

26. J. Foote, H. N. Eisen, Kinetic and affinity limits on antibodies produced during immune responses. *Proc. Natl. Acad. Sci. U. S. A.* **92**, 1254–6 (1995).